This is the authors manuscript version of the article:
A Gap-Junction Mutation Reveals That Outer Hair Cell Extracellular Receptor Potentials Drive High-Frequency Cochlear Amplification
Snezana Levic, Victoria A. Lukashkina, Patricio Simões, Andrei N. Lukashkin and Ian J. Russell
Journal of Neuroscience 19 October 2022, 42 (42) 7875-7884; DOI:
https://doi.org/10.1523/JNEUROSCI.2241-21.2022

A gap-junction mutation reveals that outer hair cell extracellular receptor potentials drive high-frequency cochlear amplification

Authors: Snezana Levic[1,2], Victoria A. Lukashkina[1], Patricio Simões[1,3], Andrei N. Lukashkin[1], Ian J. Russell[1]

[1]Sensory Neuroscience Research Group, School of Pharmacy and Biomolecular Sciences, University of Brighton, Huxley Building, Brighton BN2 4GJ, UK.

[2]Brighton and Sussex Medical School, University of Sussex, Brighton BN1 9PX, UK.

[3]Current address: School of Life Sciences, University of Sussex, Brighton BN19QG.

*Corresponding author. Email: a. lukashkin@brighton.ac.uk (A.N.L);

i.russell@brighton.ac.uk (I.J.R.)

Number of pages: 38

Number of Figures: 5

Number of words: 9335

Abstract: 245

Significance statement 114

Introduction: 586

Discussion: 1500

Conflict of Interest: The authors declare no competing interests

Acknowledgements:

Funding: This work was funded by the Medical Research Council (grant MR/W028956/1).

Short title: A mutated gap junction and cochlear amplification

Abbreviations

BM – Basilar membrane

CF – characteristic frequency

Cx26 – Connexin26

Cx30 - Connexin30

DC- Deiters' cells

EP - endocochlear potential

ERP – extracellular receptor potential

GJ – Gap junction

MET -Mechano-electrical transducer

OoC - Organ of Corti

OHC - Outer hair cell

RL – Reticular lamina

RP - Receptor potential

TM – Tectorial membrane

Abstract

Cochlear amplification enables the enormous dynamic range of hearing through amplifying cochlear responses to low-to-moderate-level sounds and compressing them to loud sounds. Amplification is attributed to voltage-dependent electromotility of mechanosensory outer hair cells (OHCs) driven by changing voltages developed across their cell membranes. At low frequencies, these voltage changes are dominated by intracellular receptor potentials (RPs). However, OHC membranes have electrical low-pass filter properties that attenuate high-frequency RPs, which should potentially attenuate amplification of high-frequency cochlear responses and impede high-frequency hearing. We made *in vivo* intracellular and extracellular electrophysiological measurements from the organ of Corti of male and female mice of the CBA/J strain, with excellent high-frequency hearing, and from the CD-1 mouse strain, which has sensitive hearing below 12 kHz, but loses high-frequency hearing within a few weeks post-partum. The CD-1 mouse strain was transfected with an A88V mutation of the connexin 30 gap-junction protein. By blocking the action of the GJ protein to reduce input resistance, the mutation increased the OHC extracellular RP (ERP) magnitude and rescued high-frequency hearing. We measured the voltage developed across the basolateral membranes of OHCs, which controls their electromotility,- for low-to-high-frequency sounds in male and female mice of the CD-1 strain that expressed the A88V mutation. We demonstrate that ERPs, not RPs, drive OHC motility and cochlear amplification at high

frequencies because, at high frequencies, ERPs are not frequency attenuated, exceed RPs in magnitude, and are appropriately timed to provide cochlear amplification.

Significance Statement

Cochlear amplification, which enables hearing's enormous dynamic range, is attributed to voltage-dependent electromotility of the mechanosensory outer hair cells (OHCs) driven by sound-induced voltage changes across their membranes. OHC intracellular receptor potentials are electrically low-pass filtered, which should hinder high-frequency hearing. We measured the intracellular and extracellular voltages that control OHC electromotility *in vivo* in a mouse strain with impaired high-frequency hearing. A gap-junction mutation of the strain rescued high-frequency hearing, increased organ of Corti resistance and preserved large OHC extracellular receptor potentials but reduced OHC intracellular receptor potentials and impaired low-frequency hearing. We concluded intracellular potentials drive OHC motility at low-frequencies and extracellular receptor potentials drive OHC motility and cochlear amplification at high-frequencies.

Key Words

Cochlea, Outer hair cells, Cochlea amplifier, Receptor potential, Connexin 30, Intracellular receptor potentials

INTRODUCTION

Cochlear amplification enables the auditory system's ten-million-fold dynamic range by amplifying cochlear responses to weak-to-moderate sounds and compressing them to loud sounds over the enormous frequency bandwidth of mammalian hearing (Robles and Ruggero, 2001). Cochlear amplification is attributed to the electromotility of three rows of sensory outer hair cells (OHCs) in the organ of Corti (OoC) that sits atop the basilar membrane (BM) (Fig. 1) (Brownell et al., 1985; Liberman et al., 2002; Ashmore, 2008; Dallos, 2008; Mellado Lagarde et al., 2008). At each location from low-frequency apex to high-frequency basal coil, the BM is tonotopically, mechanically, tuned to a place-dependent characteristic frequency (CF) where cochlear amplification is optimum (Robles and Ruggero, 2001).

OHC electromotility is driven by voltage differences generated by mechanoelectrical transducer (MET) current flow across the electrical impedance of OHC basolateral membranes (Fig. 1, OHC basolateral conductance (R_{OHCBL}) and capacitance (C_{OHCBL})) (Santos-Sacchi and Dilger, 1988), which are populated by the voltage-sensitive motor protein SLC26a5, prestin (Zheng et al., 2000). However, in addition to the limiting kinetics of prestin (Santos-Sacchi et al., 2021), the low-pass filter electrical properties of the OHC membrane ($R_{OHCBL} \times C_{OHCBL}$) attenuates the intracellular receptor potential (RP) with increasing frequency (Kössl and Russell, 1992), thereby setting an upper-frequency limit on OHC electromotility if the RP determines the electromotility driving voltage. A clue to the identity of the driving voltage for high-frequency OHC motility was provided by a discovery in a mutant of the CD-1 mouse strain. CD-1 mice display rapid-onset presbycusis (high-frequency hearing loss, Mahendrasingam et al., 2011). In contrast, the CD-1Cx30$^{A88V/A88V}$ mutant, which expresses the A88V/A88V mutation of Connexin 30 (Cx30) in the cochlea (Bosen et al., 2014; Lukashkina et al., 2017a; Kelly et al., 2019), has sensitive high-frequency hearing, although low-frequency hearing (< 12 kHz) is impaired. Cx30 contributes to the formation of large gap junctions (GJs,

Fig1A, B) (Lim, 1986; Forge et al., 2003), that interconnect, and permit bidirectional flow of ions and signalling molecules, between OoC supporting cells, including Deiters' cells (DCs) and outer pillar cells (OPCs) (Liu et al., 2009; Jagger and Forge, 2014).

Insensitive hearing for frequencies below 12 kHz may be due to the reduced endocochlear potential (EP) of CD-1Cx30$^{A88V/A88V}$ mice, which is ~60% that of mice (e.g. CBA/J strain) with sensitive high-frequency hearing (Lukashkina et al., 2017a). The EP drives the OHC MET current (Davis, 1965; Russell, 1983; Fettiplace, 2017) and EP reduction decreases cochlear sensitivity (Sewell, 1984). Thus, sensitive high-frequency hearing in CD-1Cx30$^{A88V/A88V}$ mice is surprising. A potential basis for their ability to hear high-frequency sounds arises from a discovery that the amplitudes of extracellular receptor potentials (ERPs) recorded immediately adjacent to OHCs (Fig. 1A) in CD-1Cx30$^{A88V/A88V}$ mice are similar to those of CBA/J mice (Lukashkina et al., 2017a). ERPs, unlike RPs, are not filtered by the OHC's electrical properties and do not decline in magnitude with increasing frequency.

ERPs magnitudes in CD-1Cx30$^{A88V/A88V}$ and CBA/J mice may be similar due to an increased electrical resistance of the OoC extracellular pathway in CD-1Cx30$^{A88V/A88V}$ compared with CBA/J mice. This would enable a smaller MET current flow in CD-1Cx30$^{A88V/A88V}$ mice to generate ERPs comparable to those of CBA/J mice. We measured intracellular RPs and ERPs from OHCs, and the electrical resistance between the OoC fluid spaces and scala media *in vivo.* We show how these changes account for the sensitive high-frequency responses of CD-1Cx30$^{A88V/A88V}$ mice in the face of reduced EP. Finally, we showed that ERPs are sufficient to drive cochlear amplification at high frequencies when RPs are severely attenuated by the OHC membrane time constant.

MATERIALS AND METHODS

Animal preparation

All experiments performed at the University of Brighton complied with Home Office guidelines under the Animals (Scientific Procedures) Act of 1986 and were approved by the University of Brighton Animal Welfare and Ethical Review Body. Male and female mice at 3-5 weeks of age were anesthetized with urethane (ethyl carbamate; 2 mg/g body weight i.p.) for surgical procedures at the University of Brighton. Mice were tracheotomized, and their core temperature was maintained at 38 °C. A caudal opening was made in the ventro-lateral aspect of the right bulla to reveal the round window. The right parietal and intarietal bones were firmly secured to the head holder using a stainless-steel rod and dental acrylic cement.

Electrophysiology

An Ag/AgCl ground electrode was inserted into the muscles of the neck. Intracellular electrodes (40–60 MΩ, 3 M KCl filled) were pulled from 1 mm O.D., 0.7 mm I.D. quartz glass tubing on a Sutter P-2000 micropipette puller. Signals were amplified and conditioned using laboratory-built pre-amplifiers and conditioning amplifiers that were carefully isolated and screened to avoid electromagnetic contamination from the sound system. The resistance and capacitance of the pipettes acts as a low-pass filter with a corner frequency that shifts to lower frequencies with the depth of penetration into the OoC. The frequency responses of the electrodes were, therefore, calibrated in situ according to a technique first described by (Baden-Kristensen and Weiss, 1983; Cody and Russell, 1987; Fridberger et al., 2004). The filter behaved as a single-pole low-pass filter, with 3 dB cut-off frequencies ranging from 4.5 to 9.5 kHz without capacitance compensation. Electrodes were advanced using a piezo-activated micropositioner (Marzhause GMBH). The pipette tip was inserted through the round window membrane and into the BM under visual control to a location close to the feet of the OPCs. The first cells to be encountered had resting potentials of ~ -100 mV, could be held in stable

condition for > 10 minutes and were assumed to be supporting cells. When advanced carefully forward and out of the presumed supporting cells, the electrode tip entered an extracellular space with zero potential (presumed OoC fluid spaces). When the pipette tip was further advanced by a few microns it encountered cells with resting potentials between -25 to -45 mV (presumed to be OHCs) that could be held for seconds to several minutes. The electrode tip inevitably encountered the positive potential of the fluid space of the scala media if advanced further through the presumed OHCs.

The electrical resistance between the OoC fluid space immediately adjacent to the OHC basolateral membrane and the scala media was measured by passing 100 Hz sinusoidal current from a calibrated constant current source through a micropipette. The measuring amplifier with the current source was also equipped with a bridge balancing circuit (James Hartley). Most of the micropipette resistance was bridge balanced in the OoC fluid space. This is necessary because the micropipette resistance far exceeds that of the resistance between the scala media and OoC fluid spaces and would dominate any measurements. It was not possible to bridge balance and compensate for the microelectrode resistance completely. Hence, measurements of residual unbalanced microelectrode resistance were made by passing current through the microelectrode while the electrode was still in the OoC fluid spaces. After measurements in the OoC fluid space, the micropipette tip was stepped a few microns through the reticular lamina (RL) into the scala media and the resistance measurement were repeated. The micropipette tip was then stepped back into the OoC fluid space and sinusoidal current was again passed through the tip of the micropipette to check that the micropipette unbalanced resistance remained the same. If the micropipette resistance changed, the data were discarded. The electrical resistance of the current pathway between the OoC fluid space and the scala media was calculated as a difference between the resistance measurements at these two locations. The command voltage for the current injection was software generated and the

current source was calibrated by passing it through known value resistors. A wide range of currents from $3x10^{-11}$ to $5x10^{-7}$ A was used to confirm the linearity of the electrode resistance and the passive resistance between the scala media and the OoC fluid space.

Sound system

Sound was delivered via a probe with its tip within 1 mm of the tympanic membrane and coupled to a closed acoustic system comprising two MicroTechGefell GmbH 1-inch MK102 microphones for delivering tones and a Bruel and Kjaer (www.Bksv.co.uk) 3135 0.25-inch microphone for monitoring sound pressure at the tympanum. The sound system was calibrated in situ for frequencies between 1 and 70 kHz by using a laboratory designed and constructed measuring amplifier (James Hartley), and known sound pressure levels (SPLs) were expressed in dB SPL with reference to 2×10^{-5} Pa. White noise for acoustical calibration and tone sequences for auditory stimulation were shaped with raised cosines of 0.5 ms duration were synthesized by a Data Translation 3010 (Data Translation, Marlboro, MA) data acquisition board, attenuated, and used for sound-system calibration and the measurement of electrical cochlear responses.

Experimental design and statistical analyses

Heterozygous (CD-1Cx30$^{A88V/-}$) mice were crossed to generate +/+, +/- and -/- genotypes. Male and female mice were studied in approximately equal proportions. No phenotypic differences were observed between males and females. Tests were performed on CD-1Cx30$^{A88V/A88V}$ and CBA/J mice at 3 - 5 weeks of age to standardize our measurements and to reduce animal numbers because of the ease of preparing the cochleae for measurement in this age range. Measurements were made from all CBA/J mice in a litter. Measurements could not effectively be made blind from CD-1 mice with the A88V/A88V mutation of connexin30 because homozygous (CD-1Cx30$^{A88V/A88V}$) mice have characteristically rough

coats (Bosen et al., 2014) and excellent high-frequency hearing, whereas smooth coated wild-type littermates have no high-frequency hearing and heterozygous littermates are somewhere in between (Lukashkina et al., 2017a). Even so, the tested mice were genotyped after each experiment. Experiments were terminated (< 5% of all measurements) if the physiological state of the preparation changed during a measurement in which case data from the sample were excluded. For statistical significance for a given physiological experiment, data were compared from at least 5 CBA/J and 5 CD-1Cx30$^{A88V/A88V}$ mice, obtained from recordings of 2 or 3 complete litters, that were tested before genotypes were determined. Physiological data were plotted as mean ± standard deviation (SD) using Fig P (www.figpsoft.com) or Origin 9.5 (OriginLab Corp. Northampton, MA) software. Statistical tests were performed with GraphPad Prism 8.1 (https://www.graphpad.com/quickcalcs). Statistical comparisons were made using unpaired two-tailed Student's *t*-tests for unequal variances unless otherwise noted.

Code / software

For physiological recordings, data acquisition and data analysis were performed using a PC with custom programmes written in MATLAB (MathWorks, MA). The programmes are available upon request from authors ANL and IJR. Please note that the programmes were written to communicate with specific hardware (Data Translation 3010 board and custom-made GPIB-controlled attenuators) and will need modifications to be used with different hardware. All proprietary software used in data acquisition and analysis is referred to above in the appropriate section.

RESULTS

Intracellular and extracellular cochlear electrical responses measured *in vivo*

Endocochlear potentials and low-frequency intracellular outer hair cell receptor potentials are larger in CBA/J than in CD-1Cx30$^{A88V/A88V}$ mice

When the MET channels are gated by sound-induce hair bundle displacements (Fettiplace and Hackney, 2006) (Figs. 1A, B), the OHC MET current is driven through the MET conductance by the positive EP of the scala media and the negative OHC resting membrane potential acting in series (Davis, 1965; Russell, 1983). The magnitude of these two potentials acting in tandem should largely determine the OHC RP magnitude for a given hair bundle displacement. At high frequencies, other factors will influence the OHC RP magnitude, including the OHC membrane constant.

RPs were recorded with micropipette electrodes in response to 5 kHz stimulus tones from presumed OHCs in the basal turns of CBA/J and CD-1Cx30$^{A88V/A88V}$mice. The characteristic frequencies (CFs) of the OHCs were between 52 kHz and 56 kHz. The 5 kHz stimulus frequency was chosen because it is well within the frequency bandwidth of the micropipettes (low-pass corner frequencies 7.5 – 10.5 kHz). The presumed OHCs were eventually encountered after the micropipette first penetrated the BM, then the supporting cells (presumed DCs), which have very negative resting membrane potentials that are similar in CBA/J and CD-1Cx30$^{A88V/A88V}$ mice (CBA/J: -110.3 ± 5.4 mV, n = 15; CD-1Cx30$^{A88V/A88V}$; -112.5 ± 4.2 mV, n = 17 (t = 1.26 P = 0.22, d.f. = 28)). The electrode next entered the zero potential of the OoC fluid spaces (Figs. 1A, B) and then the OHCs. Presumed OHCs were identified by their large RPs and small negative resting membrane potentials. In response to 5 kHz tones at 90 dB SLP, presumed OHC RPs recorded from sensitive CBA/J mice had peak-to-peak values of (29.2 ± 2.7 mV, n = 5) and those from CD-1Cx30$^{A88V/A88V}$mice were very significantly smaller (17.6 ± 3.8 mV, n = 7) (t = 5.8217, P = 0.0002, d.f. = 10) (Fig. 2A). Symmetry about the resting membrane potentials of the RPs, and hence the operating points of the OHC MET conductance, in the two mouse strains were very similar (Fig. 2A, inset). OHC

RPs and ERPs from CD-1Cx30$^{A88V/A88V}$ mice appear to phase lead those from CBA/J mice (Figs 2, 3) by about 15 degrees. However, the traces shown in the figures are not corrected for the microelectrode filter properties because the stimulation frequency was below the microelectrode cut-off frequency. The microelectrodes in each experiment had slightly different low cut-off frequencies and some phase shift between traces in different experiments is expected because the phase shift at the cut-off frequency is already 45°. The smaller size of the OHC RPs in CD-1Cx30$^{A88V/A88V}$ mice may be due to differences in the EP measured from the scala media in CBA/J (+112.8 ± 1.2 mV, n=12) and CD-1Cx30$^{A88V/A88V}$ (71.3 ± 2.8 mV, n = 12) mice, which are significantly different ($t = 47.19$, $P < 0.0001$, d.f. = 22) and their OHC resting membrane potentials (CBA/J mice: -39.6 ± 3.7 mV (n = 5); CD-1Cx30$^{A88V/A88V}$ mice: -29.8 ± 5.3 mV (n = 7), which are also significantly different ($t = 5.82$, $P = 0.0002$, d.f. = 10). Together the EP in series with the OHC resting membrane potential provide the driving voltage for the OHC MET current (CBA/J: 152.4 mV; CD-1Cx30$^{A88V/A88V}$: 101.1 mV) (Fig. 2B). The magnitudes of the RPs of CD-1Cx30$^{A88V/A88V}$ mice and CBA/J mice are close to the predicted values if the magnitude of the receptor current is proportional to driving voltage for the OHC MET current. However, other factors such as OHC membrane conductance and the electrochemical environment of the OHCs may also determine the magnitude of the OHC RP.

Outer hair cell extracellular receptor potentials recorded in the organ of Corti of CBA/J and CD-1Cx30$^{A88V/A88V}$ mice have similar magnitudes

OHC RPs, but not ERPs are attenuated for stimulus frequencies above the corner frequency of the OHC membrane low-pass filter ($R_{OHCBL} \times C_{OHCBL}$; Fig. 1 B; Kössl and Russell, 1992; Dallos and Evans, 1995; Fridberger et al., 2004). ERPs are dominated by the return-flow of receptor currents from the adjacent OHCs (Figs. 1 A, B). Location of the micropipette tips

in the OoC fluid spaces was finely adjusted to locate them as close as possible to the basolateral membrane of an OHC without the tips being blocked through contact with cell membranes. Further advance of the micropipettes resulted in penetration of a presumed OHC. ERPs recorded from CBA/J and CD-1Cx30$^{A88V/A88V}$ mice are not significantly different ($t = 0.60$, $P = 0.5531$, d.f. = 29) in magnitude (Fig. 2C). They are large, being maximally 17.8 mV (CBA/J: 15.8 ± 2.2 mV, n = 14) and 16.5 mV (CD-1Cx30$^{A88V/A88V}$: 15.4 ± 1.5 mV, n = 17) peak-to-peak in response to 5 kHz tones at 95 dB SPL. ERPs recorded from a CBA/J and a CD-1Cx30$^{A88V/A88V}$ mice with similar auditory sensitivities at 53 kHz are also closely similar in magnitude and sensitivity (Fig. 2D), being 0.12 ± 0.03 mV, n = 6 (CBA/J) and 0.13 ± 0.04 mV, n = 7 (CD-1Cx30$^{A88V/A88V}$) for threshold 53 kHz tones at 20 dB SPL. Thus, despite large and significant ($P < 0.001$) differences in the EP and OHC resting membrane potential (Fig. 2B) and RPs (Fig. 2A) between CBA/J and CD-1Cx30$^{A88V/A88V}$mice, ERPs are not significantly different.

Potential difference across outer hair cell basolateral membranes smaller in CD-1Cx30$^{A88V/A88V}$ than in CBA/J mice for low stimulus frequencies.

The voltage-dependent motility of OHCs is controlled by the potential difference developed across their basolateral membranes (Fig. 1, Santos-Sacchi and Dilger, 1988). This potential difference was determined for OHCs in CBA/J and CD-1Cx30$^{A88V/A88V}$ mice by subtracting the ERP from the OHC RP point-by-point in response to 5 kHz tones. Representative examples of these measurements are shown in Figs. 3A, B (CBA/J) and Figs. 3 C, D (CD-1Cx30$^{A88V/A88V}$). The same micropipette was used for each pair of measurements with the assumption that the electrical corner frequency of the micropipette and recording system did not change during the few microns excursion of the pipette tip from fluid filled OoC

space to the intracellular location and back again. The peak-to-peak transmembrane potential difference developed across the OHC basolateral membranes of the peak-to-peak responses to 95 dB SPL 5 kHz tones was significantly larger in CBA/J ($t = 10.40$, $P<0.0001$, 377 df = 10), in CBA/J mice (17.2 ± 2.6 mV, n = 5) than in CD-1Cx30A88V/A88V mice (5.2 ± 1.4 378 mV, n = 7). ERPs phase led OHC RPs by about 15 degrees (e.g. Figs. 3A, C) and the transmembrane potential difference phase led the OHC RP by 45 degrees (e.g. Figs. 3B, D). This phase difference could be due largely to phase delays in the intracellular measurements introduced by the OHC membrane time constant, which was not determined.

The electrical resistance of the current path between the organ of Corti fluid spaces and the scala media in CD-1Cx30$^{A88V/A88V}$ exceeds that in CBA/J mice

Despite OHC intracellular RPs in CD-1Cx30$^{A88V/A88V}$ mice being significantly smaller, ERPs in CD-1Cx30$^{A88V/A88V}$ and CBA/J mice are similar in magnitude. As a step towards resolving this apparent paradox, we tested the possibility that the OoC electrical properties of CD-1Cx30$^{A88V/A88V}$ mice differed from those of CBA/J mice. We measured the electrical resistance between the OoC fluid space immediately adjacent to the OHCs (Fig. 4A, R_{FS}) and common ground (Fig. 4A, Ground), which provides a measure of the resistance of the OHC MET current inward pathway. We then measured the electrical resistance between the scala media (Fig. 4A, R_{SM}) and common ground and (Fig. 4A, Ground), which provides a measure of the resistance of the OHC MET current outward pathway. We used a technique that did not rely on successfully bridge balancing the electrical resistance of the electrode in the scala tympani. We believed this to be impossible because the electrode tip has to traverse the BM, OoC, and RL to make the resistance measurements. The electrode was advanced through the OoC and the micropipette tip finely located in the OoC fluid space adjacent to an OHC without contacting a cell membrane, where the electrode was bridge balanced (Fig. 4A, black

electrode). The voltage response was then measured to a 100 Hz sinusoidal current from a calibrated constant current source, stepped in amplitude from 3 x 10^{-11} A. The relationship between injected current and voltage response provided a measure of the resistance between the fluid space (Fig. 4A, R_{FS}) and the common ground (Fig. 4A, Ground). The micropipette was then moved a few microns through the RL into the scala media (see Fig 4A, red electrode). The voltage response to the sinusoidal current was again measured to provide a measure of the resistance between scala media (Fig. 4A, R_{SM}) and the common ground (Fig. 4A, R_{FS}). The micropipette tip was again moved back into the OoC fluid space and sinusoidal current was again passed through the tip of the micropipette to check that the micropipette resistance remained the same. If the micropipette resistance changed, the data were discarded. For all currents that provided linear voltage responses, i.e., > 5 x 10^{-10} A (see Fig. 4), we obtained the resistance by dividing the voltage responses by the injected currents. Log scales are used in Figs. 4B, C to show a liner relationship (see dotted lines, slopes of 1 in Figs. 4B, C) between injected current and voltage extended over a wide range of electrical currents. Linear scales of data presented in Figs. 4B, C are used in Figs. 4D, E to show the slope resistance of the measurements. These measurements revealed the resistance of the return current pathway from the OHCs Fig. 4A, black) of both CD-1Cx30$^{A88V/A88V}$ and CBA/J mice was less than that of the inward current pathway to the OHC MET conductance (Fig. 4A, red), although, overall, these resistances appear to be greater in CD-1Cx30$^{A88V/A88V}$ than in CBA/J mice. A potential problem with this conclusion from these measurements is that there is no guarantee that the electrode resistance has been fully compensated in all measurements. The electrode resistance did not however change between measurements made in the scala media and fluid spaces made in each pair of measurements reported here. Thus, we were able to provide a measurement of the OoC fluid space resistance relative to that of the scala media and the differences in this resistance between CD-1Cx30$^{A88V/A88V}$ and CBA/J mice. We did this by subtracting the OoC

fluid space measurement from the scala media measurement because both were potentially contaminated by addition of the same uncompensated electrode resistance. The subtraction removes any uncompensated electrode resistance from the measurement. Accordingly, the resistance difference between the scala media and fluid spaces of the OoC for CBA/J mice was 280.6 ± 37.4 kΩ, n = 8 (mean ± SD), which is significantly smaller (t = 4.70, P =0.004, d.f. = 13) than that for CD-1Cx30$^{A88V/A88V}$ mice (614.2 ± 197.9 kΩ, n = 7). These findings indicate the resistive pathway of the flow of current from the OHCs, which has a major role in the determining the amplitude of the ERP (Mistrík et al., 2009), is smaller than that of the inward flow of current to the OHC MET conductance and the resistance of both pathways is significantly increased in CD-1Cx30$^{A88V/A88V}$ mice.

Extracellular receptor potentials dominate driving voltage for outer hair cells somatic motility for frequencies above 10 kHz.

In response to 5 kHz tones, the voltage generated across the basolateral membranes of presumed OHCs in the basal turn of the cochlea is larger in CBA/J mice than in CD-1Cx30$^{A88V/A88V}$ mice (Fig. 3). However, the ERPs generated at 5 kHz and 53 kHz are similar in both CBA/J and CD-1Cx30$^{A88V/A88V}$ mice with similar high-frequency cochlear sensitivity (Fig. 2D). How does the relationship between OHC intracellular and extracellular potentials, and hence the potential difference across OHC basolateral membranes, change as a function of tone frequency? Measurements were challenging and successful recordings were made in seven CD-1Cx30$^{A88V/A88V}$ mice, only two of which remained sensitive within 5 dB SPL of the initial thresholds throughout the 40-minute recording period. The others remained within 10 dB of the initial threshold (20 - 30 dB SPL). Measurements (mean of ten 70 dB SPL tone presentations for each frequency step within frequency range of 4 - 74 kHz in 2 kHz steps) were made only while the OHC membrane potential remained stable. The 70 dB SPL tone level was chosen to obtain reliable signals over a wide frequency range. This presented the problem

that it was not possible to determine the true threshold (20 – 30 dB SPL) at the CF of the recording location, so the frequency that gave the largest magnitude responses was referred to as the CF. ERP (Fig. 5A) and intracellular RP (Fig. 5B) magnitudes were plotted as functions of stimulus frequency and presented as raw (open symbols) and compensated for the low-pass filter of the recording pipette measured in situ (solid symbols) (Kössl and Russell, 1992; Fridberger et al., 2004). The superimposed intracellular RPs and ERPs compensated for the low-pass filter of the microelectrode (Figs. 5A, B, solid symbols) are shown in Fig. 5C and for another OHC in a different cochlea in Fig. 5D. Mean data from four RP/ERP sets of OHC measurements from the 64 kHz region of the same cochlea are shown in Fig. 5E. In all measurements from CD-1Cx30$^{A88V/A88V}$ mice, for frequencies below ~ 10 kHz, the magnitudes of the ERPs and intracellular RPs are similar (compare with level functions presented in Fig. 3C). For frequencies above this, the magnitude of the intracellular RP diverges from that of the ERPs with increasing frequency, presumably because of the OHC membrane time constant (Cody and Russell, 1987; Kössl and Russell, 1992). A magnitude notch (vertical dotted lines, Fig. 5) is most noticeable in the intracellular RPs. For measurements at BM frequency places with CFs between 58 kHz and 68 kHz (63.1 ± 3.2 kHz, n = 9), the tip of the notch is centred on frequencies between 42 kHz and 48 kHz (43.1 ± 3.2 kHz, n = 9), which is 0.552 ± 0.035 octaves below the CF of the recording site (or 0.683 CF frequency) when calculated independently for each of the nine measurement sites. The reduced size of the notch in extracellular recordings at 70 dB SPL may be due to spread of extracellular current from multiple sources and the frequency location of the notch could not be accurately determined in six of the ERP measurements. The RP magnitude increases sharply when the tone frequency is stepped above that of the notch and reaches a maximum close to the CF. The magnitude of the voltage response measured at the CF at 70 dB SPL, when compensated for the low-pass filter of the recording pipette, but not for the time constant of the presumed OHCs (resting membrane

potentials -35 mV ± 4 mV, n = 4) is significantly different (t =10.10, P < 0.0001, d.f. = 13) between the intracellular (0.64 mV ± 0.07 mV, n = 4) and extracellular (3.08 ± 0.47 mV, n = 11) RPs measured from the same cochleae. The potential difference generated across the presumed OHC basolateral membranes is indicated by the solid blue line in Fig. 5E, where it is minimal for frequencies below 10 kHz and closely similar to the ERP for frequencies above this. Accordingly, if OHC electromotility is controlled by the potential difference developed across the OHC basolateral membranes, the findings presented here indicate that the voltage that controls OHC electromotility is dominated by the ERP for frequencies above 10 kHz in the high-frequency region of the mouse cochlea. This finding reinforces the widely held view that hair cell and BM responses are actively amplified for frequencies at and around the CF and not in the tail region of the frequency tuning curve where the difference between the RP and ERP is minimal (Robles and Ruggero, 2001).

The phase of the 70 dB SPL iso-level ERP and RP s of frequency were similar in form between measurements in different preparations with closely similar frequency locations (Figs. 5C-E). but was seen most clearly in the averaged data of Fig 5E. The roll-off of the phase, with increasing stimulus frequency, is interrupted close to the frequency of the minimum of the magnitude notch (between 47 kHz and 50 kHz, Fig. 5, dashed vertical lines) by a phase plateau. The plateau, which lies ~ 0.5 octaves below the CF, represents a phase shift of 0.34 ± 0.04 cycles (n = 8).

DISCUSSION

Significance of intracellular and extracellular outer hair cell receptor potentials for cochlear amplification

OHC somatic electromotility, the cellular basis for cochlear amplification, is controlled cycle-by-cycle (Dewey et al., 2021) by the potential difference developed across OHC basolateral membranes (Santos-Sacchi and Dilger, 1988) during cochlear sound stimulation (Ashmore, 2008; Dallos, 2008; Mellado Lagarde et al., 2008). A clue as to how high-frequency cochlear amplification is achieved was provided by the CD-1Cx30$^{A88V/A88V}$ mouse. The wild-type CD-1 mouse has sensitive low-frequency hearing and early-onset high-frequency loss. The mutation reverses this situation. The CD-1Cx30$^{A88V/A88V}$ mouse has poor low-frequency, but excellent high-frequency hearing (Bosen et al., 2014; Lukashkina et al., 2017a; Kelly et al., 2019) similar to that of the CBA/J mouse with excellent overall hearing. Critical for our investigation, we measured potential differences across OHC basolateral membranes *in vivo*. These measurements in the high-frequency cochlear region, revealed RPs dominate OHC transmembrane potentials to 5 kHz tones. At 5 kHz, RPs are barely attenuated by the OHC membrane time constant (Kössl and Russell, 1992; Johnson et al., 2011). The transmembrane potential difference at 5 kHz in CD-1Cx30$^{A88V/A88V}$ is smaller than in CBA/J mice due to reduced RP driving voltage in CD-1Cx30$^{A88V/A88V}$ mice (Lukashkina et al., 2017a). If this situation pertains to OHCs in the 5 kHz cochlear location, it could account for why the low-frequency (<12 kHz) auditory sensitivity of CD-1Cx30$^{A88V/A88V}$ mice is poor compared to wild-type CD-1 littermates. For frequencies above 12 kHz, the OHC transmembrane voltage at the cochlear base becomes dominated by the extracellular ERP (Fig 5), which has similar magnitude in CBA/J and CD-1Cx30$^{A88V/A88V}$ mice.

Is the ERP sufficient to drive OHC motility and cochlear amplification at high frequencies? Prestin-based OHC electromotility has been shown to be essential for cochlear amplification (Ashmore 2008; Dallos, 2008), including in the high-frequency, sensitive, mouse cochlea (Weddell et al., 2011). Close to hearing threshold (~ 20 dB SPL, Taberna and Liberman, 2005; Russell et al., 2007; Ren et al., 2016) in the 50 kHz – 60 kHz region of the

sensitive mouse cochlear, CF tones displace the BM by 0.2 nm and the ERP is 0.13 mV. Intracellular RP at 53 kHz was below the measurement noise floor at 20 dB SPL and estimated to be ~0.01 mV through extrapolation. Thus, the OHC transmembrane potential is 0.12 mV and the ERP-BM displacement gain at CF is 1.6 nm/mV. How does this value of gain compare with estimates obtained elsewhere? The measurements are similar to an ERP-BM gain of 3 nm/mV derived from published measurements (Kössl and Russell, 1992; Russell et al., 1995; Sellick et al., 1983) in the 16-18 kHz region of the guinea pig cochlea and 1.7nm/mV for ERP-BM gain at 50 kHz derived from measurements of OHC nonlinear capacitance (Santos-Sacchi and Tan, 2021; Fig. 5, Santos-Sacchi personal communication). According to Dewey et al. (2021), the *in vivo* amplitude of OHC electromotility at CF, is four times the BM vibration amplitude. From the ERP-BM gain reported above, this provides OHC-ERP gains of 7.2 nm/mV for mice at 53 kHz and 12 nm/mV for guinea pigs at 16-18 kHz. These gain values compare with 10 – 20 nm/mV for the electromotility gain of large, isolated, apical guinea pig OHCs (Ashmore, 1987). We propose, therefore, given the limitations of comparing OHCs operating within the constraints of the OoC with low-frequency movements of isolated OHCs, the ERP is capable of controlling high-frequency cochlear amplification in the mouse cochlea.

Significance of cochlear partition resistance for outer hair cell extracellular receptor potential magnitude

Although having a strongly reduced EP (Figs. 1, 4A), hence, reduced OHC MET current and RPs compared with CBA/J mice, the ERPs of CD-1Cx30$^{A88V/A88V}$ and CBA/J mice are similar in size and sensitivity to sound stimulation. This might be because the electrical resistance across the RL between the scala media and OoC fluid space (Fig. 4) in CD-1Cx30$^{A88V/A88V}$ mice is over double that in CBA/J mice. Increased resistance between the

scala media and OoC fluid space should enable a given current flow to generate a larger voltage drop across this resistance in CD-1Cx30$^{A88V/A88V}$ than in CBA/J mice. We suggest the resistance increase is due to altered current pathways within the OoC contributed partially or entirely by altered electrophysiological properties of DCs and interconnecting GJs in CD-1Cx30$^{A88V/A88V}$ mice.

Receptor potential iso-level response notch, tectorial membrane, and timing of cochlear amplification

The timing of the relative movement of structures within the cochlear partition is critical for cochlear amplification. To be effective, OHC voltage-dependent forces, controlled by the ERPs at high frequencies, as demonstrated in this study, and fed back to the cochlear partition, should be in phase with BM velocity (Nilsen and Russell, 1999). At frequencies and levels where they are most effective, forces generated by the OHCs can enhance the BM's motion 10000-fold at threshold (Robles and Ruggero, 2001). Timing of OHC excitation is determined by the relative movement between the RL, from which stereocilia, the mechanosensitive organelles of the OHCs protrude, and the TM in which the stereocilia are imbedded. There is substantial theoretical, indirect, and direct evidence to support the hypothesis that the TM coupled to the OoC acts as a resonant structure which determines the timing of the delivery of OHC electromotility that is critical for cochlear amplification (Allen, 1980; Zwislocki, 1980; Gummer et al., 1996; Lukashkin and Russell, 2003; Lukashkin et al., 2007; Meaud and Grosh, 2010; Lukashkin et al., 2012). The amplitude notch and associated phase jump in the ERPs and intracellular RPs recorded from OHCs reported here (Fig. 5), which occurs about a half octave below the CF, supports earlier (Lukashkin et al., 2010) and current findings (Nankali et al., 2020) about multimodal vibrations involving the TM. The frequency of the amplitude notch indicates the first mode of the TM/OoC complex vibrations (frequently referred to as a TM resonance (Allen, 1980;

Zwislocki, 1980)) when the radial shear between the TM and RL is minimal, hence, minimizing the OHC excitation and producing a local minimum of the OHC RPs and ERPs. At this frequency, as reported here, ERPs show an advance in phase of ~ 0.3 cycles, which would introduce the correct phase relationship between mechanical and electrical responses of the cochlea to enable cochlear amplification (Nilsen and Russell, 1999). Indeed, at this frequency and above, the amplitudes and phases of OHC and BM responses show the level-dependent properties associated with cochlear amplification (Kössl and Russell, 1992; Russell et al., 1995). The notch in the iso-level, frequency, OHC RP function (Fig. 5) is more sharply tuned than when measured extracellularly, when it becomes increasingly broader and less distinct with increasing levels (Nankali et al., 2020). We attribute this difference to the level-dependent increasing numbers of generators (OHCs) contributing to the extracellular signal (Patuzzi et al., 1989) that smears the phase data rather than to damping by fluid in the subtectorial space, as has been recently suggested and modelled based on cochlear microphonic measurements (Nankali et al., 2020).

We demonstrated that the ERP dominates the driving voltage for OHC somatic motility at the CF in the basal, high-frequency region of the mouse cochlea (Fig. 5). Intracellular RP, however, dominates the driving voltage when the same cochlear region is stimulated with frequencies below the cut-off frequency of the OHC membrane (Fig. 2A). If the last observation is true for the low-frequency cochlear apex, and the intracellular RP dominates the driving voltage for the OHC somatic motility in this region, it implies very different phase relationships (probably close to counter phasic) between the OHC excitation and force generation and amplification mode at the base and apex of the mouse cochlea (Lukashkina et al., 2017b). Attempts to relate OHC intracellular and extracellular measurements to the movements of the BM have been made (Russell et al., 1995; Fridberger et al., 2004), but the measurements reported here, and others made previously in the guinea

pig cochlea (Russell and Kossl, 1992; Fridberger et al., 2004) emphasise the importance of comparing intracellular OHC RPs and ERPs with measurements from the other OoC structures and from the TM (Ren et al., 2016; Cooper et al., 2018; Dewey et al., 2018; He et al., 2018; Motallebzadeh et al., 2018; Ren and He, 2020) to discover their relative contribution to the passive mechanics, amplification and frequency tuning in the cochlea.

Cochlear amplification mechanisms may differ between the cochlear apex and base, possibly because OoC supporting cells may dominantly influence the mechanics and electrochemistry of OHCs in the stiffer basal turns than in the apex (Russell, 2014; Lukashkina et al., 2017b; Lukashkina et al., 2022). Significantly, the transition frequency from RP to ERP as the dominant control-voltage for OHC electromotility coincides with that proposed for the transition of OHCs generating amplification through isotonic length changes to reciprocal isometric interaction with the cochlear partition (Lukashkina et al., 2017b). At these high frequencies, the ERP, and hence cochlear amplification, is influenced by the electrochemical and mechanical consequences of the interaction between OHCs and structures of the OoC (Lukashkina et al., 2022) to form a potential feedback mechanism.

REFERENCES

Allen JB (1980) Cochlear micromechanics-A physical model of transduction. *Journal of the Acoustical Society of America* 68:1660-1670.

Ashmore JF (1987) A fast motile response in guinea-pig outer hair cells: the cellular basis of the cochlear amplifier. *The Journal of Physiology* 388:323-47.

Ashmore J (2008) Cochlear Outer Hair Cell Motility. *Physiological Review* 88:173-210.

Baden-Kristensen K, Weiss TF (1983) Receptor potentials of lizard hair cells with free-standing stereocilia: responses to acoustic clicks. *The Journal of Physiology* 335:699-721.

Bosen F, Schütz M, Beinhauer A, Strenzke N, Franz T, Willecke K (2014) The Clouston syndrome mutation connexin30 A88V leads to hyperproliferation of sebaceous glands and hearing impairments in mice. *FEBS Letters* 588:1795-1801.

Brownell WE, Bader CR, Bertrand D, de Ribaupierre Y (1985) Evoked mechanical responses of isolated cochlear outer hair cells. *Science* 227:194-196.

Cody AR, Russell IJ (1987) The response of hair cells in the basal turn of the guinea-pig cochlea to tones. *The Journal of Physiology* 383:551-569.

Cooper NP, Vavakou A, van der Heijden M (2018) Vibration hotspots reveal longitudinal funneling of sound-evoked motion in the mammalian cochlea. *Nature Communications* 9:3054.

Dallos P (2008) Cochlear amplification, outer hair cells and prestin. Curr Opin Neurobiol 18:370-376.

Dallos P, Evans BN (1995) High-frequency motility of outer hair cells and the cochlear amplifier. *Science* 267:2006-2009.

Davis H (1965) A Model for Transducer Action in the Cochlea. *Cold Spring Harbor Symposium for Quantatative Biology* 30:181-190.

Dewey JB, Xia A, Müller U, Belyantseva IA, Applegate BE, Oghalai JS (2018) Mammalian Auditory Hair Cell Bundle Stiffness Affects Frequency Tuning by Increasing Coupling along the Length of the Cochlea. *Cell Reports* 23:2915-2927.

Dewey JB, Altoè A, Shera CA, Applegate BE, Oghalai JS (2021) Cochlear outer hair cell electromotility enhances organ of Corti motion on a cycle-by-cycle basis at high frequencies in vivo. Proceedings of the National Academy of Sciences U S A 118(43):e2025206118.

Dong W, Varavva P, Olson ES (2013) Sound transmission along the ossicular chain in common wild-type laboratory mice. *Hearing Research* 301:27-34.

Fettiplace R (2017) Hair Cell Transduction, Tuning, and Synaptic Transmission in the Mammalian Cochlea. In: *Comprehensive Physiology*, pp 1197-1227.

Fettiplace R, Hackney CM (2006) The sensory and motor roles of auditory hair cells. *Nature Reviews Neuroscience* 7:19-29.

Forge A, Becker D, Casalotti S, Edwards J, Marziano N, Nevill G (2003) Gap junctions in the inner ear: Comparison of distribution patterns in different vertebrates and assessement of connexin composition in mammals. *Journal of Comparative Neurology* 467:207-231.

Fridberger A, de Monvel JB, Zheng J, Hu N, Zou Y, Ren T, Nuttall A (2004) Organ of Corti Potentials and the Motion of the Basilar Membrane. *The Journal of Neuroscience* 24:10057-10063.

Gummer AW, Hemmert W, Zenner HP (1996) Resonant tectorial membrane motion in the inner ear: its crucial role in frequency tuning. *Proceedings of the National Academy of Sciences* 93:8727-8732.

He W, Kemp D, Ren T (2018) Timing of the reticular lamina and basilar membrane vibration in living gerbil cochleae. *eLife* 7:e37625.

Jagger DJ, Forge A (2014) Connexins and gap junctions in the inner ear – it's not just about K+ recycling. *Cell and Tissue Research* 360:633-644.

Johnson Stuart L, Beurg M, Marcotti W, Fettiplace R (2011) Prestin-Driven Cochlear Amplification Is Not Limited by the Outer Hair Cell Membrane Time Constant. *Neuron* 70:1143-1154.

Kelly JJ, Abitbol JM, Hulme S, Press ER, Laird DW, Allman BL (2019) The connexin 30 A88V mutant reduces cochlear gap junction expression and confers long-term protection against hearing loss. *Journal of Cell Science* 132.

Kössl M, Russell IJ (1992) The phase and magnitude of hair cell receptor potentials and frequency tuning in the guinea pig cochlea. *The Journal of Neuroscience* 12:1575-1586.

Liberman MC, Gao J, He DZZ, Wu X, Jia S, Zuo J (2002) Prestin is required for electromotility of the outer hair cell and for the cochlear amplifier. *Nature* 419:300-304.

Lim DJ (1986) Functional structure of the organ of Corti: a review. Hearing Res 22:117-146.

Liu W, Boström M, Kinnefors A, Rask-Andersen H (2009) Unique expression of connexins in the human cochlea. *Hearing Research* 250:55-62.

Lukashkin AN, Russell IJ (2003) A second, low-frequency mode of vibration in the intact mammalian cochlea. *Journal of the Acoustical Society of America* 113:1544-1550.

Lukashkin AN, Smith JK, Russell IJ (2007) Properties of distortion product otoacoustic emissions and neural suppression tuning curves attributable to the tectorial membrane resonance. J*ournal of the Acoustical Society of America* 121:337.

Lukashkin AN, Richardson GP, Russell IJ (2010) Multiple roles for the tectorial membrane in the active cochlea. *Hearing Research* 266:26-35.

Lukashkin AN, Legan PK, Weddell TD, Lukashkina VA, Goodyear RJ, Welstead LJ, Petit C, Russell IJ, Richardson GP (2012) A mouse model for human deafness DFNB22 reveals that hearing impairment is due to a loss of inner hair cell stimulation. *Proceedings of the National Academy of Sciences* 109:19351-19356.

Lukashkina VA, Levic S, Lukashkin AN, Strenzke N, Russell IJ (2017a) A connexin30 mutation rescues hearing and reveals roles for gap junctions in cochlear amplification and micromechanics. *Nature Communications* 8:14530.

Lukashkina VA, Yamashita T, Zuo J, Lukashkin AN, Russell IJ (2017b) Amplification mode differs along the length of the mouse cochlea as revealed by connexin 26 deletion from specific gap junctions. *Scientific Reports* 7:5185.

Lukashkina VA, Levic S, Simões P, Xu Z, DiGuiseppi JA, Zuo J, Lukashin AN, Russell IJ (2022) *In vivo* optogenetics reveals control of cochlear electromechanical responses by supporting cells. *Journal of Neuroscience* JN-RM-2127-21.

Mahendrasingam S, MacDonald JA, Furness DN (2011) Relative Time Course of Degeneration of Different Cochlear Structures in the CD/1 Mouse Model of Accelerated Aging. *Journal of the Association for Research in Otolaryngology* 12:437-453.

Meaud J, Grosh K (2010) The effect of tectorial membrane and basilar membrane longitudinal coupling in cochlear mechanics. *The Journal of the Acoustical Society of America* 127:1411-1421.

Mei L, Chen J, Zong L, Zhu Y, Liang C, Jones RO, Zhao H-B (2017) A deafness mechanism of digenic Cx26 (GJB2) and Cx30 (GJB6) mutations: Reduction of endocochlear potential by impairment of heterogeneous gap junctional function in the cochlear lateral wall. *Neurobiological Disorders* 108:195-203.

Mellado Lagarde MM, Drexl M, Lukashkina VA, Lukashkin AN, Russell IJ (2008) Outer hair cell somatic, not hair bundle, motility is the basis of the cochlear amplifier. *Nature Neuroscience* 11:746-748.

Mistrík P, Mullaley C, Mammano F, Ashmore J (2009) Three-dimensional current flow in a large-scale model of the cochlea and the mechanism of amplification of sound. *Journal of The Royal Society Interface* 6:279-291.

Motallebzadeh H, Soons JAM, Puria S (2018) Cochlear amplification and tuning depend on the cellular arrangement within the organ of Corti. *Proceedings of the National Academy of Sciences* 115:5762-5767.

Nankali A, Wang Y, Strimbu CE, Olson ES, Grosh K (2020) A role for tectorial membrane mechanics in activating the cochlear amplifier. *Scientific Reports* 10:17620.

Nilsen KE, Russell IJ (1999) Timing of cochlear feedback: spatial and temporal representation of a tone across the basilar membrane. *Nature Neuroscience* 2:642-648.

Patuzzi RB, Yates GK, Johnstone BM (1989) The origin of the low-frequency microphonic in the first cochlear turn of guinea-pig. *Hearing Research* 39:177-188.

Ren T, He W (2020) Two-tone distortion in reticular lamina vibration of the living cochlea. *Communications Biology* 3:35.

Ren T, He W, Kemp D (2016) Reticular lamina and basilar membrane vibrations in living mouse cochleae. *Proceedings of the National Academy of Sciences* 113:9910-9915.

Robles L, Ruggero MA (2001) Mechanics of the Mammalian Cochlea. *Physiological Review* 81:1305-1352.

Russell IJ (1983) Origin of the receptor potential in inner hair cells of the mammalian cochlea--evidence for Davis' theory. *Nature* 301:334-336.

Russell IJ (2014) Roles for Prestin in Harnessing the Basilar Membrane to the Organ of Corti. In: Insights from Comparative Hearing Research (Köppl C, Manley GA, Popper AN, Fay RR, eds), pp37–67. Springer New York.

Russell I, Kössl M (1992) Modulation of hair cell voltage responses to tones by low-frequency biasing of the basilar membrane in the guinea pig cochlea. The *Journal of Neuroscience* 12:1587-1601.

Russell IJ, Kössl M, Murugasu E (1995) A comparison between tone-evoked voltage responses of hair cells and basilar membrane displacements recorded in the basal turn of the guinea pig cochlea. In: Advances in Hearing Research (Manley GA, Klump GM, Köppl C, Fastl H, Oeckinghaus H, eds), pp 136-144. Singapore: World Scientific.

Russell IJ, Legan PK, Lukashkina VA, Lukashkin AN, Goodyear RJ, Richardson GP (2007) Sharpened cochlear tuning in a mouse with a genetically modified tectorial membrane. *Nature Neuroscience* 10:215-23.

Santos-Sacchi J, Dilger JP (1988) Whole cell currents and mechanical responses of isolated outer hair cells. *Hearing Research* 35:143-150.

Santos-Sacchi J, Tan WJT (2021) Coupling between outer hair cell electromotility and prestin sensor charge depends on voltage operating point. *Hearing Research* doi: 10.1016/j.heares.2021.108373.

Santos-Sacchi J, Navaratnam D, Tan WJT (2021) State dependent effects on the frequency response of prestin's real and imaginary components of nonlinear capacitance. *Scientific Reports* 9;11(1):16149. doi: 10.1038/s41598-021-95121-4

Sellick PM, Patuzzi R, Johnstone BM (1983) Comparison between the tuning properties of inner hair cells and basilar membrane motion. *Hearing Research* 10:93-100.

Sewell WF (1984) The effects of furosemide on the endocochlear potential and auditory-nerve fiber tuning curves in cats. *Hearing Research* 14:305-314.

Taberner AM, Liberman MC (2005) Response properties of single auditory nerve fibers in the mouse. *Journal of Neurophysiology* 93:557-69.

Weddell TD, Mellado-Lagarde M, Lukashkina VA, Lukashkin AN, Zuo J, Russell IJ (2011) Prestin links extrinsic tuning to neural excitation in the mammalian cochlea. *Current Biology* 21:R682-3.

Zheng J, Shen W, He DZ, Long KB, Madison LD, Dallos P (2000) Prestin is the motor protein of cochlear outer hair cells. *Nature* 405:149-155.

Zwislocki JJ (1980) Theory of cochlear mechanics. *Hearing Research* 2:171-182.

Acknowledgments:

Funding: This work was funded by the Medical Research Council grant MR/N004299/1.

Author contributions: I.J.R., and A.N. L. conceived the research. I.J.R., A.N.L. and S.L. designed the research. performed and analyzed ex vivo physiological measurements. A.N.L. wrote computer programs. V.A.L., S. L, P.S. and I.J.R. performed and analyzed physiological recordings. A.N.L. and I.J.R. wrote the paper with significant input from S.L. and P.S.

Competing interests: The authors declare that they have no competing interests. **Data and materials availability:** All data needed to evaluate the conclusions in the paper are present in the paper. Additional data related to this paper may be requested from the authors.

FIGURE CAPTIONS

Figure 1. Schematic cross sections the cochlea and OHC MET current pathway. A, recording arrangement for OHC RP measurements and ERP measurements from fluid spaces bounded by the OHCs (blue), DCs (orange) with phalangeal processes extending to OHC apical surface and the RL. Inner hair cells (red), pillar cells (black), basilar membrane (BM), tectorial membrane (TM). ChR2 activating wide blue laser beam and interferometer red laser beams are shown. Schematic of inward and return pathways of MET current (continuous red dashed line) driven by the in-series batteries of the positive EP and negative OHC resting membrane potential. **B**. Details of MET current flow in the OoC from the scala media, through the OHC MET conductance (OHC_{MET}). This is gated due to radial shear displacement (B. Radial arrows) between the TM and RL caused by transverse displacement of the BM (B. Transverse arrow). MET current passes out via the OHC basolateral conductance (R_{OHCBL}) and capacitance (C_{OHCBL}), which introduce a low-pass limiting time-constant ($R_{OHCBL} \times C_{OHCBL}$), through the

fluid space, into the DCs, through the GJs to the stria vascularis (the source of the EP) returning through the OHC Met conductance to complete the circuit.

Figure 2. OHC intracellular receptor potential (OHC RP) magnitudes are larger in CBA/J than in CD-1Cx30$^{A88V/A88V}$mice but ERPs are similar. **A**. Mean ± SD of the magnitude of presumed OHC intracellular RPs as functions of SPL for responses to 5 kHz tones from five CBA/J mice and seven CD-1Cx30$^{A88V/A88V}$ mice. Inset: examples of intracellular RP waveforms in response to 5 kHz tones at 90 dB SPL about the resting membrane potential. Resting potentials: CBA/J, -41 mV; CD-1Cx30$^{A88V/A88V}$, -28 mV. **B**. Mean ± SD of positive EP (solid bar) and presumed negative OHC resting membrane potentials (hatched bar) for CBA/J (black) and CD-1Cx30$^{A88V/A88V}$ (red) mice. * indicates significantly different ($P < 0.001$). **C.** Mean ± SD of ERP magnitude from five CBA/J and five CD-1Cx30$^{A88V/A88V}$ mice in response to stimulation with 5 kHz tones as a function of SPL. **D**. Representative examples of the magnitude of ERP from CBA/J and CD-1Cx30$^{A88V/A88V}$ mice in response to stimulation with 5 kHz tones (closed symbols) and 53 kHz (open symbols) as a function of SPL. Inset: examples of ERP wave forms in response to 5 kHz, 90 dB SPL tones about the zero potential of the fluid space (dotted line). Measurements were taken from mice with similar auditory sensitivity at 53 kHz. 53kHz data compensated for low-pass electrode characteristics (6 dB octave^{-1}, corner frequencies: 7.4 kHz, CBA/J; 9.0 kHz, CD-1Cx30$^{A88V/A88V}$ mouse).

Figure 3. Potential difference across OHC basolateral membranes is larger for 5 kHz tones in CBA/J mice (A, B) than in CD-1Cx30$^{A88V/A88V}$ (C, D) mice. A, C. Magnitude and phase of presumed OHC RP and ERPs. **B, D.** Examples of waveforms recorded, in response to 5 kHz, 90 dB SPL tones, OHC RP (black), ERP (red), transmembrane potential difference

(blue) for CBA/J mice (**B**) and CD-1Cx30$^{A88V/A88V}$ mice (**D**). Insets: Schematic of recording locations and symbol and colour key. Magnitude and phase measurements were not compensated for low-pass electrode characteristics which had corner frequencies < 8.5 kHz.

Figure 4. Electrical resistance of inward and outward MET current pathways is larger in CD-1Cx30$^{A88V/A88V}$ than in CBA/J mice. A. Schematic of inward current flow through the OHC MET conductance (red) and outward current flow from the OHC basolateral conductances (black) and resistive electrical network in a limited cross-section of the OoC. **B, C.** Examples for CBA/J mice (B) and CD-1Cx30$^{A88V/A88V}$ mice (C) of voltage measured (average of 20 presentations) in response to current injected through the almost bridge-balance circuit when the micropipette tip is in the OoC fluid space next to a presumed OHC (black square; A, R_{FS}) and in the scala media (red square; A, R_{SM}). Log-log plots show linearity of measurement. Dotted lines in A and B: slope of one. Resistance between the scala media and the OoC fluid space calculated as the difference between resistance measurements in these two locations. **D, E.** Linear representations of data in B, C to show slope resistance.

Figure 5. Extracellular receptor potentials dominate driving voltage for the outer hair cell somatic motility for tone frequencies above 10 kHz. Examples of magnitudes and phases of ERPs (red symbols and lines) and OHC RPs (black symbols and lines) as a function of stimulus tone frequency recorded in response to 70 dB SPL tones presented in 2 kHz steps from 4 kHz to 74 kHz. **A**. ERPs recorded in the fluid space close to an OHC of a CD-1Cx30$^{A88V/A88V}$ mouse with a CF of 62 kHz. Open symbols: raw data. Solid symbols: data corrected for recording electrode low-pass filter characteristics (solid black line). **B**. Magnitude of OHC RPs recorded from a presumed OHC immediately adjacent to recording in (**A**) (resting

membrane potential – 31 mV) as a function of stimulus frequency. Open symbols: raw data. Closed symbols: data compensated for recording electrode low-pass filter characteristics. **C**. Superimposed, compensated data from (**A**) and (**B**) together with ERP and RP phase (lines, no symbols). **D**. ERP, RPs and their phases from another OHC in a different cochlea. **E**. Mean ± SD of four intracellular OHC RPs and four ERP recordings made immediately adjacent to the intracellular recordings in the 64 kHz frequency region of a single cochlea of a CD-1Cx30$^{A88V/A88V}$ mouse. Thick blue line: potential difference across presumed OHC basolateral membranes (difference between mean magnitudes of ERP and intracellular RP). Mean phase (line, no symbols) ± SD (dotted lines) for the ERPs and OHC RPs. Vertical solid lines: CF; dotted line: notch minimum peak frequency. All data from CD-1Cx30$^{A88V/A88V}$ mice with ERP thresholds < 30 dB SPL at the CF. Phase was corrected for middle ear transfer characteristics (Dong et al., 2013), sound system and recording electrode. Dotted lines (**A**, **B**): recording noise floors.

FIGURES

Figure 1

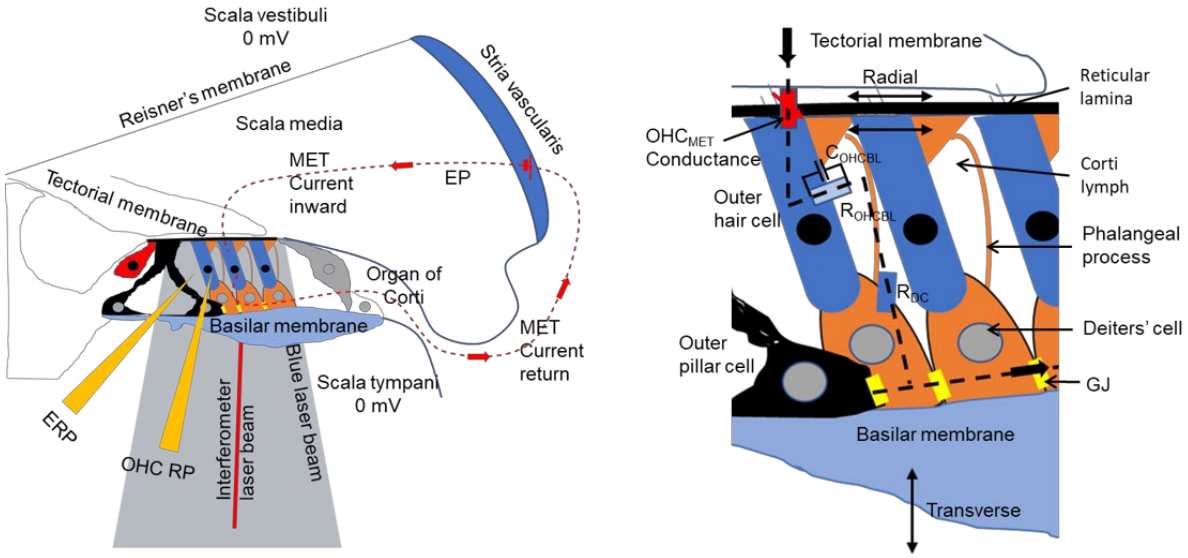

Figure 2

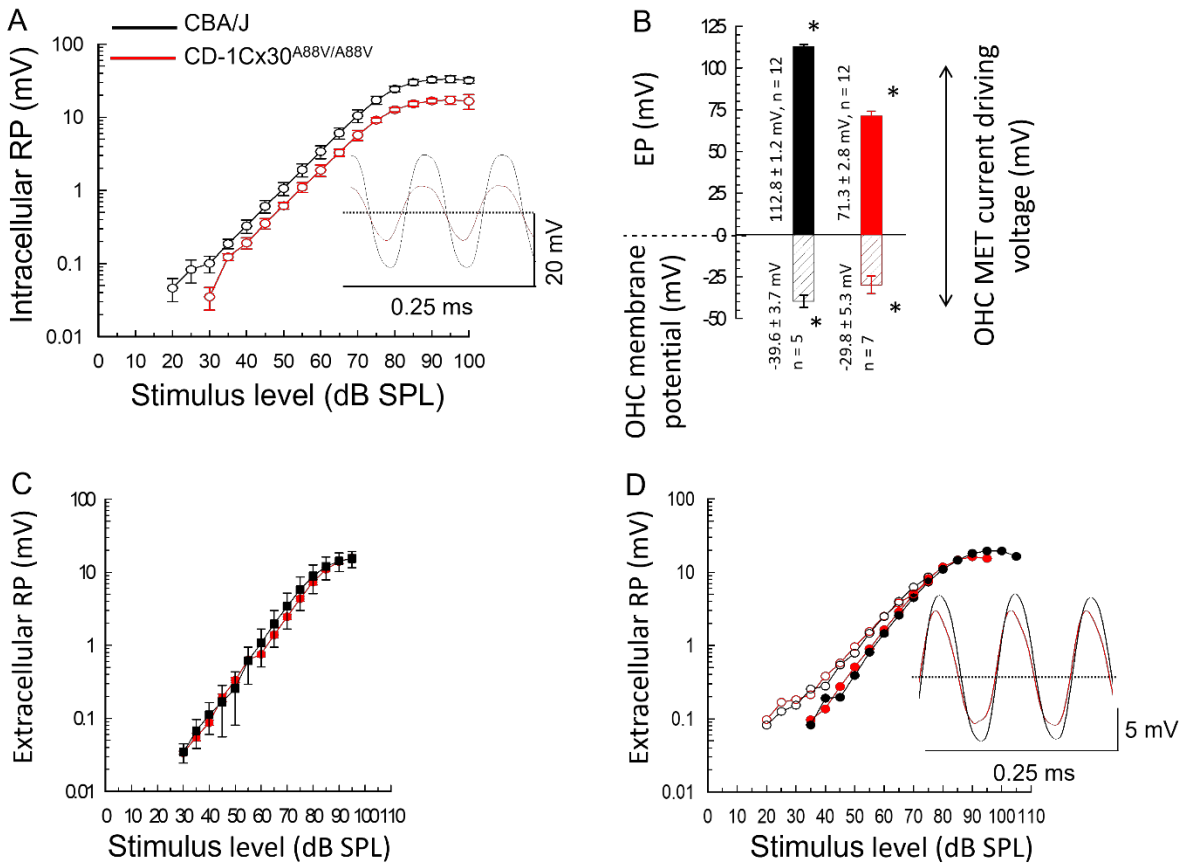
A
CBA/J
CD-1Cx30A88V/A88V
Intracellular RP (mV)
100
10
1
0.1
0.01
0 10 20 30 40 50 60 70 80 90 100
Stimulus level (dB SPL)
20 mV
0.25 ms
B
EP (mV)
OHC membrane potential (mV)
125
100
75
50
25
0
-25
-50
112.8 ± 1.2 mV, n = 12
71.3 ± 2.8 mV, n = 12
-39.6 ± 3.7 mV
n = 5
-29.8 ± 5.3 mV
n = 7
OHC MET current driving voltage (mV)
C
Extracellular RP (mV)
100
10
1
0.1
0.01
0 10 20 30 40 50 60 70 80 90 100110
Stimulus level (dB SPL)
D
Extracellular RP (mV)
100
10
1
0.1
0.01
0 10 20 30 40 50 60 70 80 90 100110
Stimulus level (dB SPL)
5 mV
0.25 ms

Figure 3

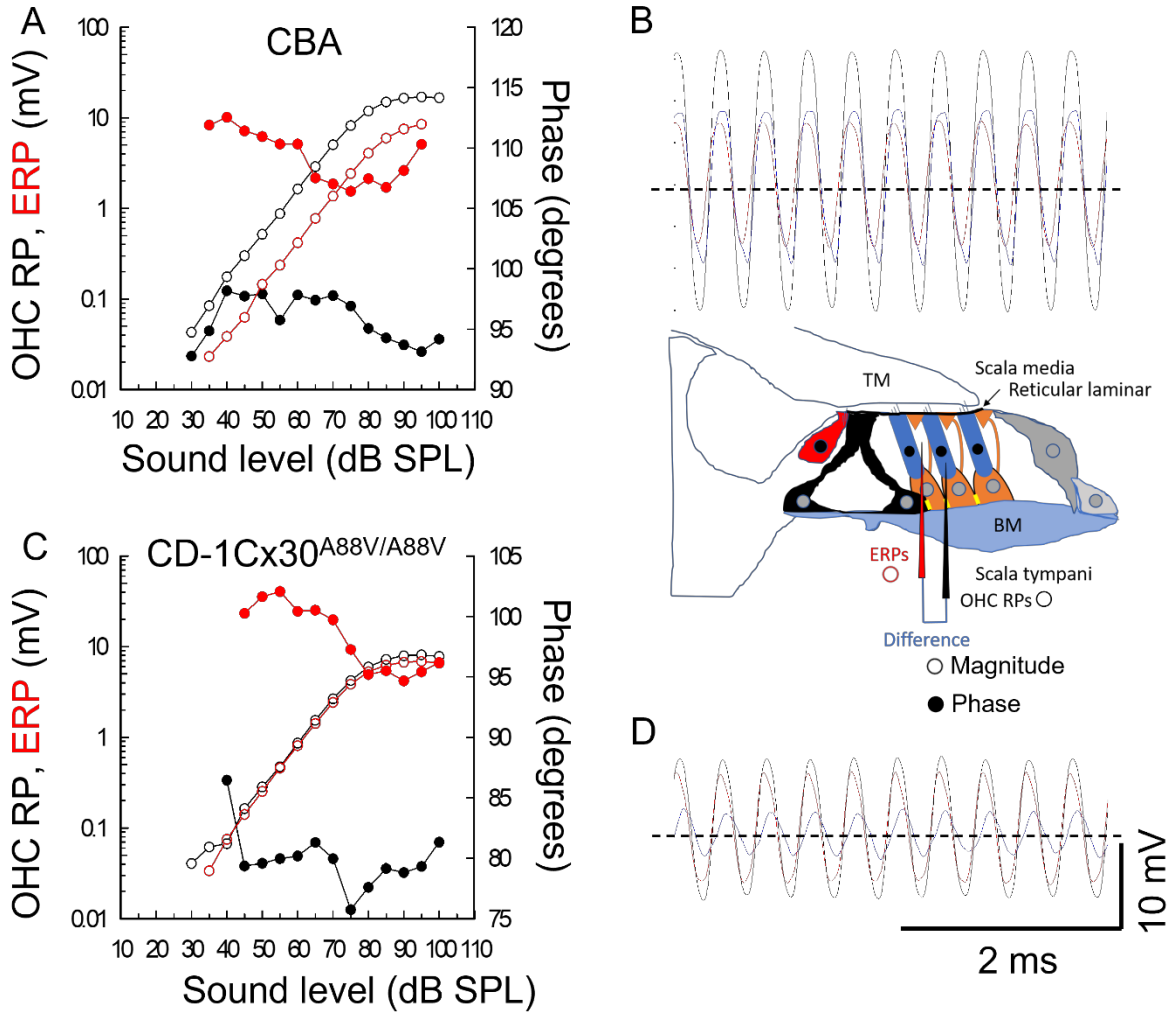
A
CBA
OHC RP, ERP (mV)
Phase (degrees)
Sound level (dB SPL)
C
CD-1Cx30A88V/A88V
OHC RP, ERP (mV)
Phase (degrees)
Sound level (dB SPL)
B
TM
Scala media
Reticular laminar
BM
ERPs
Scala tympani
OHC RPs
Difference
Magnitude
Phase
D
10 mV
2 ms

Figure 4

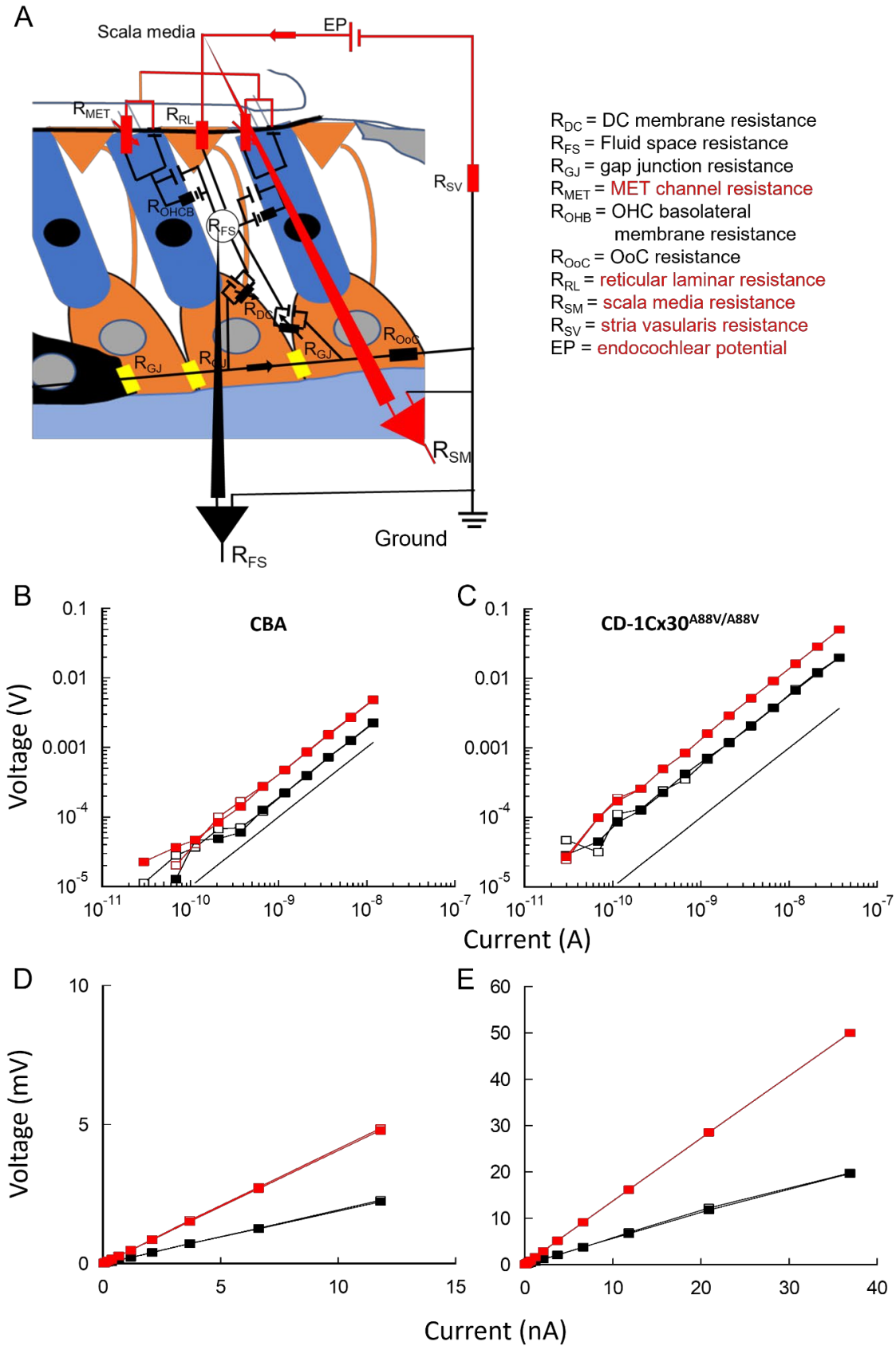
A
Scala media
EP
R_{MET}
R_{RL}
R_{SV}
R_{OHCB}
R_{FS}
R_{DC}
R_{OoC}
R_{GJ}
R_{GJ}
R_{GJ}
R_{SM}
Ground
R_{FS}
R_{DC} = DC membrane resistance
R_{FS} = Fluid space resistance
R_{GJ} = gap junction resistance
R_{MET} = MET channel resistance
R_{OHB} = OHC basolateral membrane resistance
R_{OoC} = OoC resistance
R_{RL} = reticular laminar resistance
R_{SM} = scala media resistance
R_{SV} = stria vasularis resistance
EP = endocochlear potential
B
CBA
C
CD-1Cx30$^{A88V/A88V}$
Voltage (V)
Current (A)
D
E
Voltage (mV)
Current (nA)

Figure 5

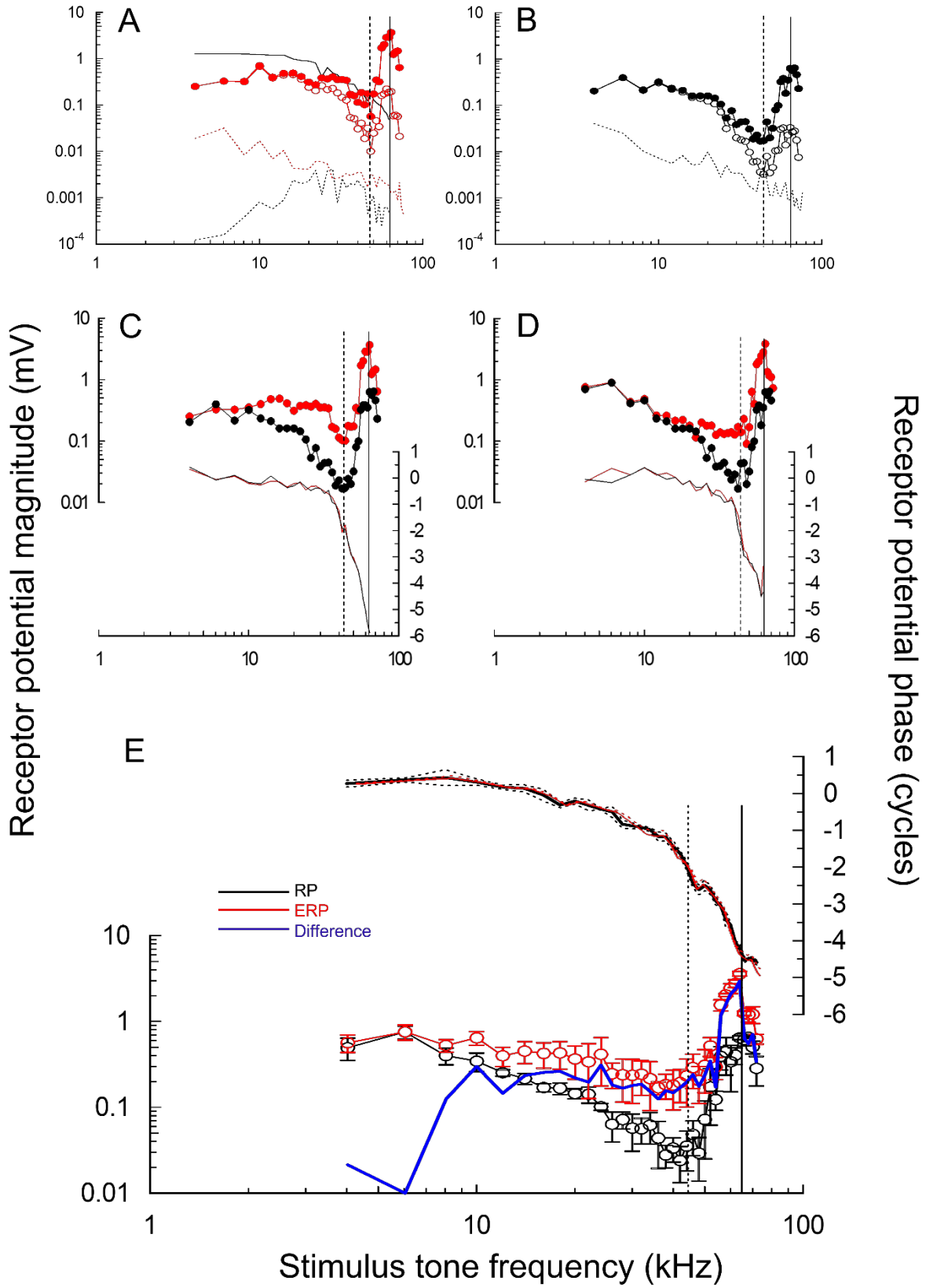
A
B
C
D
E
RP
ERP
Difference
Receptor potential magnitude (mV)
Receptor potential phase (cycles)
Stimulus tone frequency (kHz)